

Continuous Macroscopic Limit of a Discrete Stochastic Model for Interaction of Living Cells

Mark Alber,^{1,*} Nan Chen,¹ Pavel M. Lushnikov,^{2,3} and Stuart A. Newman⁴

¹*Department of Mathematics, University of Notre Dame, Notre Dame, Indiana 46656, USA*

²*Department of Mathematics and Statistics, University of New Mexico, Albuquerque, New Mexico 87131, USA*

³*Landau Institute for Theoretical Physics, Kosygin Street 2, Moscow, 119334, Russia*

⁴*Department of Cell Biology and Anatomy, New York Medical College, Valhalla, New York 10595, USA*

(Received 1 March 2007; published 19 October 2007)

We derive a continuous limit of a two-dimensional stochastic cellular Potts model (CPM) describing cells moving in a medium and reacting to each other through direct contact, cell-cell adhesion, and long-range chemotaxis. All coefficients of the general macroscopic model in the form of a Fokker-Planck equation describing evolution of the cell probability density function are derived from parameters of the CPM. A very good agreement is demonstrated between CPM Monte Carlo simulations and a numerical solution of the macroscopic model. It is also shown that, in the absence of contact cell-cell interactions, the obtained model reduces to the classical macroscopic Keller-Segel model. A general multiscale approach is demonstrated by simulating spongy bone formation, suggesting that self-organizing physical mechanisms can account for this developmental process.

DOI: 10.1103/PhysRevLett.99.168102

PACS numbers: 87.18.Ed, 05.40.Jc, 05.65.+b, 87.18.Hf

A large literature exists studying continuous limits of pointwise discrete microscopic models for biological systems. For example, the classic Keller-Segel partial differential equation (PDE) model of chemotaxis [1] was derived from a discrete model with pointwise cells undergoing a random walk [2–5]. However, many biological phenomena require taking into account the finite size of biological cells, and much less work has been done on deriving macroscopic limits of microscopic models which treat cells as extended objects. The mesoscopic cellular Potts model (CPM), first introduced by Glazier and Graner [6,7], has been used as a component of multiscale, experimentally motivated hybrid approaches, combining discrete and macroscopic continuous representations, to simulate, among others, morphological phenomena in the cellular slime mold *Dictyostelium discoideum* [8], vascular development [9] and the proximo-distal increase in the number of skeletal elements in the developing avian limb [10].

One of the earliest attempts at combining mesoscopic and macroscopic levels of a description of cellular dynamics was described in Ref. [11], where the diffusion coefficient for a collection of noninteracting randomly moving cells was derived from a one-dimensional CPM. Recently, a microscopic limit of a subcellular elements model [12] was derived in the form of an advection-diffusion PDE for cellular density. In previous papers [13,14], we studied the continuous limit of 1D and 2D models of individual cell motion in a medium, in the presence of an external field but without contact cell-cell interactions.

This Letter describes a derivation of the continuous macroscopic limit of the 2D CPM with contact cell-cell interactions and cell-cell adhesion which can be extended to three dimensions. Because of the fast calculation speed possible with the continuous model, we quickly test a wide parameter range and determine appropriate values for parameters used in the CPM simulations. The continuous

model provides very good approximations for a system containing a biologically realistic (i.e., large) number of cells, for which numerical simulations of CPM trajectories can be prohibitive. We demonstrate that the multiscale approach can be applied to studying biological phenomena in which a nonconfluent population of cells interact directly and via soluble factors, forming an open network structure. Examples include vasculogenesis [9,15–17] and the formation of trabecular or spongy bone [18–20].

In the CPM, defined on a multidimensional lattice, an integer vector index is associated with each lattice site (*pixel*). Each cell or medium is represented by a cluster of pixels with the same index. Indexes of pixels evolve according to the classical Monte Carlo (MC) algorithm based on Boltzmann statistics and the effective energy

$$E = E_{\text{ECM}} + E_{\text{adhesion}} + E_{\text{perimeter}} + E_{\text{field}}. \quad (1)$$

If a proposed change in a lattice configuration results in energy change ΔE , it is accepted with probability

$$\Phi(\Delta E) = 1 - \{1 - \exp[-\beta\Delta E]\}\Theta(\Delta E), \quad (2)$$

where $1/\beta$ represents an effective boundary fluctuation amplitude of model cells in units of energy and Θ is a Heaviside step function. Since the cells' environment is highly viscous, cells move to minimize their total energy consistent with imposed constraints and boundary conditions. If a change of a randomly chosen pixel's index causes cell-cell overlap, it is abandoned (due to the excluded volume constraint). Otherwise, the acceptance probability (2) is used for determining whether a pixel changes its index, which might result in changing the location of the center of mass and the dimensions of a cell. We model rectangular cells moving or changing their shapes by adding or removing a row or column of pixels (see Fig. 1). We assume that cells can come into direct contact and that they interact over long distances through

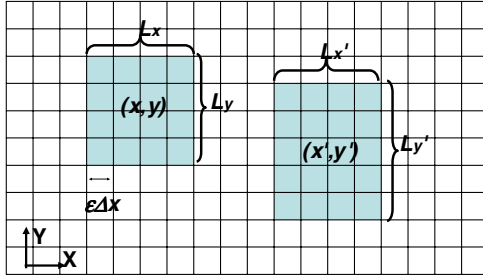


FIG. 1 (color online). Cell representation in the 2D CPM. In this picture, gray and white are used to indicate the cell body and ECM, respectively. The cell can grow or shrink in the x and y directions by adding or removing one row (or column) of pixels.

chemotaxis. E_{ECM} and E_{adhesion} in the Hamiltonian (1) phenomenologically describe the net adhesion or repulsion between the cell surface and extracellular matrix (ECM) and cell-cell adhesion: $E_{\text{ECM}} = 2J_{\text{ECM}}(L_x + L_y)$ and $E_{\text{adhesion}} = J_a L_{\text{contact}}$, respectively, where J_{ECM} and J_a are binding energies per unit length of an interface. L_{contact} is

$$\begin{aligned} P(\mathbf{r}, \mathbf{L}, t + \Delta t) = & \sum_{j=1}^2 \left[\left[\frac{1}{2} - \Omega_{j,l} \left(\mathbf{r} - \frac{\epsilon}{2} \mathbf{e}_j, \mathbf{L} + \epsilon \mathbf{e}_j; \mathbf{r}, \mathbf{L}, t \right) - \Omega_{j,r} \left(\mathbf{r} + \frac{\epsilon}{2} \mathbf{e}_j, \mathbf{L} + \epsilon \mathbf{e}_j; \mathbf{r}, \mathbf{L}, t \right) - \Omega_{j,l} \left(\mathbf{r} + \frac{\epsilon}{2} \mathbf{e}_j, \mathbf{L} - \epsilon \mathbf{e}_j; \mathbf{r}, \mathbf{L}, t \right) \right. \right. \\ & - \Omega_{j,r} \left(\mathbf{r} - \frac{\epsilon}{2} \mathbf{e}_j, \mathbf{L} - \epsilon \mathbf{e}_j; \mathbf{r}, \mathbf{L}, t \right) \left. \right] P(\mathbf{r}, \mathbf{L}, t) + \Omega_{j,l} \left(\mathbf{r}, \mathbf{L}; \mathbf{r} + \frac{\epsilon}{2} \mathbf{e}_j, \mathbf{L} - \epsilon \mathbf{e}_j, t \right) P \left(\mathbf{r} + \frac{\epsilon}{2} \mathbf{e}_j, \mathbf{L} - \epsilon \mathbf{e}_j, t \right) \\ & + \Omega_{j,r} \left(\mathbf{r}, \mathbf{L}; \mathbf{r} - \frac{\epsilon}{2} \mathbf{e}_j, \mathbf{L} - \epsilon \mathbf{e}_j, t \right) P \left(\mathbf{r} - \frac{\epsilon}{2} \mathbf{e}_j, \mathbf{L} - \epsilon \mathbf{e}_j, t \right) + \Omega_{j,l} \left(\mathbf{r}, \mathbf{L}; \mathbf{r} - \frac{\epsilon}{2} \mathbf{e}_j, \mathbf{L} + \epsilon \mathbf{e}_j, t \right) \\ & \times P \left(\mathbf{r} - \frac{\epsilon}{2} \mathbf{e}_j, \mathbf{L} + \epsilon \mathbf{e}_j, t \right) + \Omega_{j,r} \left(\mathbf{r}, \mathbf{L}; \mathbf{r} + \frac{\epsilon}{2} \mathbf{e}_j, \mathbf{L} + \epsilon \mathbf{e}_j, t \right) P \left(\mathbf{r} + \frac{\epsilon}{2} \mathbf{e}_j, \mathbf{L} + \epsilon \mathbf{e}_j, t \right) \Big]. \end{aligned} \quad (3)$$

Here we introduce dynamics into the MC algorithm by defining the time step Δt . Individual biological cells experience diffusion (see, e.g., [21]). We choose Δt to match the experimental diffusion coefficient. Equation (3) would determine a version of a kinetic or dynamic MC algorithm (see, e.g., [22]) if we were to allow fluctuation of Δt . For simplicity, we assume that $\Delta t = \text{const}$. Also, $\Omega_{j,l(r)}(\mathbf{r}, \mathbf{L}; \mathbf{r}', \mathbf{L}', t)$ denote probabilities of transitions from a cell of length L' and center of mass at \mathbf{r}' to a cell of dimensions L and center of mass at \mathbf{r} . Subscripts l and r correspond to transition by addition (removal) of a row (column) of pixels from the rear (lower) and front (upper) ends of a cell, respectively.

We define $\Omega_{j,l(r)}(\mathbf{r}, \mathbf{L}; \mathbf{r}', \mathbf{L}') \equiv T_{l(r)}(\mathbf{r}, \mathbf{L}; \mathbf{r}', \mathbf{L}') \times [1 + \phi_{j,l(r)}(\mathbf{r}, \mathbf{L}, t)]$, where $T_{l(r)}(\mathbf{r}, \mathbf{L}; \mathbf{r}', \mathbf{L}')$ denote probabilities of transitions from a cell of length L' and center of

the contact area between cells, and $E_{\text{perimeter}}$ defines an energy penalty function for dimensions of a cell deviating from the target values $L_{T_{x(y)}}$: $E_{\text{perimeter}} = \lambda_x(L_x - L_{T_x})^2 + \lambda_y(L_y - L_{T_y})^2$, where λ_x and λ_y are Lagrange multipliers. Cells can move up or down gradients of both diffusible chemical signals (*chemotaxis*) and insoluble ECM molecules (*haptotaxis*) described by $E_{\text{field}} = \mu c(\mathbf{r}, t)L_x L_y$, $\mathbf{r} = (x, y)$, where $c(\mathbf{r}, t)$ is a local concentration of signaling molecules in the extracellular space and μ is an effective chemical potential.

Let $P(\mathbf{r}, \mathbf{L}, t)$ denote the probability density for a cell with its center of mass at \mathbf{r} to have dimensions $\mathbf{L} \equiv (L_x, L_y)$ at time t . Let $\epsilon \Delta r \times \epsilon \Delta r$ be the size of a lattice site with $\epsilon \ll 1$, and let vectors $\mathbf{e}_{1,2}$ indicate changes in x and y dimensions: $\mathbf{e}_1 = \Delta r(1, 0)$, $\mathbf{e}_2 = \Delta r(0, 1)$. We normalize the total probability to the number of cells: $\int P(\mathbf{r}, \mathbf{L}, t) d\mathbf{r} d\mathbf{L} = N$. The excluded volume constraint implies that position \mathbf{r}' and size \mathbf{L}' of any neighboring cell should satisfy $2|x - x'| \geq L_x + L'_x$, $2|y - y'| \geq L_y + L'_y$.

A discrete stochastic cellular dynamics under these conditions is described by the following master equation:

mass at \mathbf{r}' to a cell of dimensions \mathbf{L} and center of mass at \mathbf{r} without taking into account the excluded volume principle. According to the CPM, we have that $T_{l(r)}(\mathbf{r}, \mathbf{L}; \mathbf{r}', \mathbf{L}') = \frac{1}{8} \Phi[E(\mathbf{r}, \mathbf{L}) - E(\mathbf{r}', \mathbf{L}')]$, where the factor of 1/8 is due to the fact that there are potentially 8 possibilities for increasing or decreasing of $L_{x(y)}$. The second term $\phi_{j,l(r)}(\mathbf{r}, \mathbf{L}, t)$ takes into account contact interactions between cells. It includes contributions from 3 possible types of stochastic jump processes due to contact interactions between cells: (a) a cell adheres to another one, (b) two adhered cells dissociate from each other due to membrane fluctuations, and (c) membranes of two adhered cells are prevented from moving inside each other (due to the excluded volume constraint) resulting in a negative sign of a contribution to a jump probability. Neglect of triple and higher order “collisions” between cells results in

$$\begin{aligned} \phi_{j,k}(\mathbf{r}, \mathbf{L}; \mathbf{r}', \mathbf{L}', t) = & (1 - N^{-1})(\epsilon \Delta r)^4 \sum_{\mathbf{L}'', \mathbf{r}''} \Theta(L_{j+1} + L''_{j+1} - 2|r''_{j+1} - r_{j+1}|) P(\mathbf{r}'', \mathbf{L}'', t) \{ \delta_{2s(r_j - r''_j), L_j + L''_j} \delta_{2s(r'_j - r''_j), L'_j + L''_j + 2\epsilon} \\ & + \delta_{2s(r_j - r''_j), L_j + L''_j + 2\epsilon} \delta_{2s(r'_j - r''_j), L'_j + L''_j} - \delta_{2s(r_j - r''_j), L_j + L''_j - 2\epsilon} \delta_{2s(r'_j - r''_j), L'_j + L''_j} \}, \end{aligned} \quad (4)$$

where δ is a Kronecker’s symbol, $s = 1$ for $k = l$, $s = -1$ for $k = r$, $L_{1(2)} = L_{x(y)}$, $L_3 = L_x$, $r_{1(2)} = x(y)$, and $r_3 = x$. The factor $(N - 1)/N$ is due to pairwise cellular interactions, and the sum of 3 terms inside parentheses corresponds to processes (a), (b), and (c), respectively.

We found by using MC simulations (not shown) that solutions of the master equation (3) with general initial conditions quickly converge to $P(\mathbf{r}, \mathbf{L}, t) = P_{\text{Boltz}}(\mathbf{r}, \mathbf{L}, t)p(\mathbf{r}, t)$, where $P_{\text{Boltz}}(\mathbf{r}, \mathbf{L}, t) = Z(\mathbf{r}, t)^{-1} \times \exp(-\beta\Delta E_{\text{length}})$ is a Boltzmann-like distribution depending on \mathbf{r} and t only through $c(\mathbf{r}, t)$, $\Delta E_{\text{length}} = E(\mathbf{r}, \mathbf{L}) - E_{\min} = \lambda_x \tilde{L}_x^2 + \lambda_y \tilde{L}_y^2 + \tilde{L}_x \tilde{L}_y \mu c(\mathbf{r}, t)$, and $\tilde{\mathbf{L}} = \mathbf{L} - \mathbf{L}^{(\min)}$ (see also [13]). Here $E_{\min} = E(\mathbf{r}, \mathbf{L}^{(\min)})$ is the minimal value of (1) achieved at $\mathbf{L} = \mathbf{L}^{(\min)}$ and $Z(\mathbf{r}, t) = (2\epsilon\Delta r)^2 \sum_{\mathbf{L}} \exp(-\beta\Delta E_{\text{length}}) \approx 2\pi/\beta\sqrt{4\lambda_x\lambda_y - \mu^2 c(\mathbf{r}, t)^2}$ is an asymptotic formula for a partition function as $\epsilon \rightarrow 0$.

The typical fluctuations of cell dimensions $\tilde{L}_{x(y)}$ are determined by $\beta\lambda_{x(y)}\tilde{L}_{x(y)}^2 \sim 1$. Suppose x_0 (y_0) are typical scales of P with respect to x (y), meaning that $x_0 \gg \tilde{L}_x$, $y_0 \gg \tilde{L}_y$. We assume that $\beta x_0^2 \lambda_x \gg 1$ and $\beta y_0^2 \lambda_y \gg 1$. We also assume that $c(\mathbf{r}, t)$ is a slowly varying function of \mathbf{r} on a scale of the typical cell's length, meaning that $x_c/L_x \gg 1$, $y_c/L_y \gg 1$, where x_c (y_c) are typical scales for variation of $c(\mathbf{r}, t)$ in x (y). We also make the additional biologically relevant assumption that $4\lambda_x\lambda_y \gg \mu^2 c(\mathbf{r}, t)^2$, meaning that a change of the typical cell size due to chemotaxis $\delta L_{x(y)}^{(\text{chemo})}$ is small: $|\delta L_{x(y)}^{(\text{chemo})}| \ll L_{x(y)}^{(\min)}$. Under all of the above mentioned assumptions, the master equation (3) is transformed in the limit $\epsilon \ll 1$ and by using Kramers-Moyal expansion [23] terminating at the second order term to the Fokker-Planck equation for $P(\mathbf{r}, \mathbf{L}, t)$. It is then reduced with the help of $P_{\text{Boltz}}(\mathbf{r}, \mathbf{L}, t)$ (see also Ref. [14]) to the evolution equation for the cellular probability density $p(\mathbf{r}, t)$

$$\begin{aligned} \partial_t p &= D_2 \partial_{\mathbf{r}}^2 p - \chi_0 \partial_{\mathbf{r}}[p \partial_{\mathbf{r}} c(\mathbf{r}, t)] + \frac{D_2}{2}(1 - N^{-1}) \\ &\quad \times [\partial_x[\psi_x p] + \partial_y[\psi_y p]], \\ \psi_{r_j} &= \int_{-L_{j+1}^{(\min)}}^{L_{j+1}^{(\min)}} \exp[\beta J_a(L_{j+1}^{(\min)} - |r'_{j+1}|)] [p(\mathbf{r} + \mathbf{e}_{j+1} r'_{j+1} \\ &\quad + \mathbf{e}_j L_j^{(\min)}) - p(\mathbf{r} + \mathbf{e}_{j+1} r'_{j+1} - \mathbf{e}_j L_j^{(\min)})] dr'_{j+1}, \end{aligned} \quad (5)$$

where $D_2 = (\epsilon\Delta r)^2/16\Delta t$, $\partial_{\mathbf{r}}^2 = \partial_x^2 + \partial_y^2$, $\chi_0 = -D_2\mu\beta L_x^{(\min)}L_y^{(\min)}$, $L_{x(y)}^{(\min)} = L_{T_{x(y)}} - J_{\text{cm}}/\lambda_{x(y)}$, and $\int p(\mathbf{r}) d\mathbf{r} = N$. Without cell-cell adhesion $J_a = 0$, Eq. (5)

describes contact cell-cell interaction with the excluded volume constraint. Last, we couple Eq. (5) to an equation describing the evolution of the chemotactic field c

$$\partial_t c = D_c \partial_{\mathbf{r}}^2 c - \gamma c + ap, \quad (6)$$

where D_c , γ , and a are diffusion, decay, and cellular production rates of the chemical, respectively. If $p(\mathbf{r}, t)$ is slow with respect to a space variable in comparison with cell length, then Eq. (5) is reduced to a simpler local PDE:

$$\partial_t p = D_2 \partial_{\mathbf{r}}^2 p - \chi_0 \partial_{\mathbf{r}}[p \partial_{\mathbf{r}} c(\mathbf{r}, t)] + D_3 \partial_{\mathbf{r}}^2 p^2, \quad (7)$$

$D_3 = D_2(1 - N^{-1})L_x^{(\min)}[\exp(\beta J_a L_x^{(\min)}) - 1]/(\beta J_a)$. We assumed for simplicity that $L_x^{(\min)} = L_y^{(\min)}$.

If contact cell-cell interactions are not taken into account (i.e., $\psi_j = 0$), Eqs. (5) and (6) reduce to the classical Keller-Segel system [1] which has a finite time singularity and which was used for modeling aggregation of bacterial colonies [24]. Contact interactions $\psi_j \neq 0$ significantly slow down collapse, and, therefore, Eqs. (5) and (6) can be used for a much longer period of time. The spongy bone formation considered in this Letter is accompanied by secretion of a viscous ECM (see below) which progressively solidifies and thereby stabilizes a transient or metastable arrangement of cells into a persistent microanatomy and therefore also prevents collapse.

Figure 2 demonstrates a very good agreement between a typical CPM with cell-cell adhesion simulations and the numerical solution of the continuous model (5) and (6). Both simulations were performed on a rectangular domain $0 \leq x, y \leq 100$ with simulation time $t_{\text{end}} = 400$. We used no-flux boundary conditions with $\Delta r = 1$, $L_{T_{x(y)}} = 3$, $\lambda_{x(y)} = 1.5$, $J_a = -0.042$, $J_{\text{cm}} = 2$, $\beta = 15$, $\mu = 0.1$, $D_c = 3.0$, $\gamma = 0.00025$, $a = 0.2$, $\Delta t = 0.0001$, and $\epsilon = 0.01$. The discretization of (6) was used to simulate $c(\mathbf{r}, t)$ on a 200×200 lattice with the time step $\Delta t_c = 0.0125$ and initial chemical field chosen in the form of $c_0(x, y) = [(x - 70)^2 + (y - 60)^2]/400$. The typical size of the mesh used in the continuous model was 1000×1000 , and the time step was 0.000625. A large number of CPM simulations have been run to guarantee a representative statistical ensemble. At each time step each cell releases chemical content $a\Delta t_c$, which is then distributed to the four nearest chemical lattice sites.

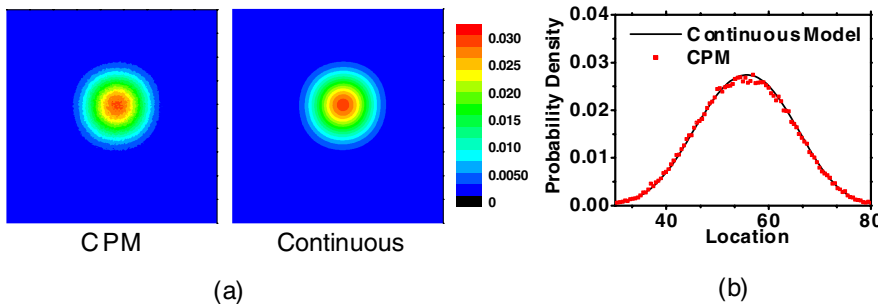


FIG. 2 (color online). Comparison between CPM and the macroscopic continuous model. (a) Plot of a 2D probability density distributions for a CPM simulation of 15 cells with $\epsilon = 0.01$ and a numerical solution $p(x, y, t)$ of the continuous equation (5). (b) Cross sections of $p(53.0, y, t)$ as functions of y for MC (squares) and continuous (solid line) simulations.

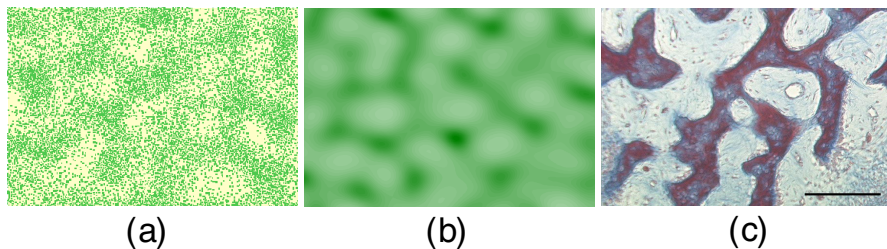


FIG. 3 (color online). Simulations of spongy bone formation. $\Delta r = 1$, $L_{T_{x(y)}} = 0.6$, $\lambda_{x(y)} = 1.5$, $J_a = 0$, $J_{cm} = 0.002$, $\beta = 15$, $\mu = -0.1$, $D_c = 0.5$, $\gamma = 0.014$, $\Delta t_c = 0.01$, $\epsilon = 0.1$, and $t_{end} = 180$, with periodic boundary conditions. (a) CPM simulation of 15 000 cells initially randomly distributed in a domain $0 \leq x, y \leq 100$ with $a = 0.7$. (b) Numerical solution of the continuous model with a uniform initial cell density distribution, 5% random fluctuation, and $a = 0.2$. (c) Histological section of developing spongy bone in the rat skull. Trichrome stain. Photographed from a section in the New York Medical College Histology slide collection. The magnification of this image is about 2 \times that of (a) and (b). Scale bar: 0.1 mm.

Now we illustrate the efficacy of our approach by modeling the formation of spongy bone via the intramembranous route. In this developmental phenomenon, which generates portions of the skull, maxilla, and mandible in vertebrate organisms, bone cells, or osteoblasts, differentiate directly from loosely packed mesenchymal cells. The differentiating cells secrete TGF- β , which acts chemotactically, influencing cell migration while simultaneously inducing production of ECM [25], which in developing bone is termed osteoid [18]. Depending on local conditions, including initial cell density, the bone will progress to a dense state or stop at a spongy state, in which bony rods or trabeculae form a Swiss-cheese-like network [see Fig. 3(c)] that eventually contains marrow tissue originating from the circulation. Our simulations, which start with initially dilute populations of cells, result in a transiently appearing set of interconnected multicellular trabeculae [see Figs. 3(a) and 3(b)] similar to the experimental picture [Fig. 3(c)]. In particular, in the simulations and the developing tissue there are many nodes from which three branches extend but few with larger numbers.

In summary, we have derived a macroscopic continuous model (5) from a mesoscopic 2D CPM and coupled it to chemoattractant equation (6). Simulations confirm a very good agreement between the CPM and macroscopic equations. Establishing a continuous limit for the CPM, which is widely used for modeling multicellular systems, should have broad applicability in biophysics. In particular, it facilitates parameter search and estimation of qualitative behaviors of large numbers of cells in implementations of the classic CPM. Numerical analysis of the macroscopic model resulted in determination of conditions promoting the formation of a latticelike aggregation pattern and allowed us to determine the parameter ranges then used in the CPM simulations of intramembranous development of spongy bone (Fig. 3). In contrast to earlier suggestions that the trabecular arrangement of spongy bone is based on preexisting vascular patterns [26] or later-forming patterns of mineral deposition [19,20], our results suggest that it can arise from the self-organizing behavior of mesenchymal cells interacting with their ECM.

This work was partially supported by NSF Grants No. 04.6071/NIH 1R0-GM076692-01, No. IBN-0344647, No. FIBR-0526854, and No. MRI DBI-0420980.

*malber@nd.edu

- [1] E. F. Keller and L. A. Segel, *J. Theor. Biol.* **30**, 225 (1971).
- [2] W. Alt, *J. Math. Biol.* **9**, 147 (1980).
- [3] H. G. Othmer and A. Stevens, *SIAM J. Appl. Math.* **57**, 1044 (1997).
- [4] A. Stevens, *SIAM J. Appl. Math.* **61**, 172 (2000).
- [5] T. J. Newman and R. Grima, *Phys. Rev. E* **70**, 051916 (2004).
- [6] F. Graner and J. A. Glazier, *Phys. Rev. Lett.* **69**, 2013 (1992).
- [7] J. A. Glazier and F. Graner, *Phys. Rev. E* **47**, 2128 (1993).
- [8] A. F. M. Marée and P. Hogeweg, *Proc. Natl. Acad. Sci. U.S.A.* **98**, 3879 (2001).
- [9] R. M. H. Merks *et al.*, *Dev. Biol.* **289**, 44 (2006).
- [10] R. Chaturvedi *et al.*, *J. R. Soc. Interface* **2**, 237 (2005).
- [11] S. Turner *et al.*, *Phys. Rev. E* **69**, 021910 (2004).
- [12] T. J. Newman, *Math. Biosci. Eng.* **2**, 611 (2005).
- [13] M. Alber *et al.*, *Phys. Rev. E* **73**, 051901 (2006).
- [14] M. Alber *et al.*, in *Single Cell Based Models in Biology and Medicine*, edited by A. R. A. Anderson *et al.* (Birkhauser-Verlag, Basel, Switzerland, 2007), pp. 53–76.
- [15] P. A. Rupp *et al.*, *Development* (Cambridge, U.K.) **131**, 2887 (2004).
- [16] A. Szabo *et al.*, *Phys. Rev. Lett.* **98**, 038102 (2007).
- [17] A. Gamba *et al.*, *Phys. Rev. Lett.* **90**, 118101 (2003).
- [18] D. H. Cormack and A. W. Ham, *Ham's Histology* (Lippincott, New York, 1987).
- [19] B. Courtin *et al.*, *Acta Biotheoretica* **43**, 373 (1995).
- [20] Z. Tabor *et al.*, *Phys. Rev. E* **66**, 051906 (2002).
- [21] J. P. Rieu *et al.*, *Biophys. J.* **79**, 1903 (2000).
- [22] A. B. Bortz *et al.*, *J. Comput. Phys.* **17**, 10 (1975).
- [23] C. W. Gardiner, *Handbook of Stochastic Methods for Physics, Chemistry, and the Natural Sciences* (Springer-Verlag, Berlin, 2004).
- [24] M. P. Brenner *et al.*, *Nonlinearity* **12**, 1071 (1999).
- [25] R. A. Kanaan and L. A. Kanaan, *Med. Sci. Monitor* **12**, RA164 (2006).
- [26] A. I. Caplan and D. G. Pechak, *Bone and Mineral Research*, edited by W. A. Peck (Elsevier, New York, 1987), p. 117.